Fourier transform to analyse reaction-diffusion dynamics in a microsystem†‡

André Estévez-Torres,[a] Thomas Le Saux,[a] Charlie Gosse,*[b] Annie Lemarchand,[c] Anne Bourdoncle[a] and Ludovic Jullien*[a]

Received 29th October 2007, Accepted 11th April 2008
First published as an Advance Article on the web 23rd May 2008
DOI: 10.1039/b805412f

An integrated approach relying on a microsystem is introduced to easily extract, from a single experiment and with a global robust bi-exponential fit, an extensive set of thermodynamic, kinetic, and diffusion parameters governing associations in solution.

Introduction

Molecular assemblies of two (or more) components are of major significance in Chemistry and Biology.[1] To describe them, thermodynamics (*e.g.* the association constant) is fundamental but dynamic properties (*e.g.* rate constants, diffusion coefficients) are also important as they convey a rich body of information. In particular, a precise knowledge of the latter parameters is essential to achieve highly selective analyses or separations.[2]

Only a few 'integrated' approaches such as Fluorescence Correlation Spectroscopy (FCS)[3] or Fluorescence Recovery After Photobleaching (FRAP)[4] may directly provide an extensive collection of rate constants and diffusion coefficients from a single experiment. Yet, although elegant, powerful, and non-invasive, these techniques suffer from demanding requirements (concentration of interacting components, nature of the fluorescent probes, range of accessible rate constants, complex data treatments).

Several microsystems (*e.g.* T-sensors) have recently been introduced to enlarge the pool of integrated approaches for *in vitro* applications.[5] They are conceptually related to FRAP as one observes reactive and diffusive processes acting together to relax out-of-equilibrium concentration profiles. While less constraining than the previously mentioned fluorescence techniques, these microfluidic devices have, to date, only been used to measure a single dynamic parameter per experiment.

We recently retained the basic principle of the preceding microsystems to characterise non-reactive binary mixtures by analysis of their diffusive behavior.[6] In the present account, we extend our analysis and show that our chip design and protocol for data processing are particularly favourable to easily extract, from a single experiment, an extensive set of thermodynamic, kinetic, and diffusion parameters governing associations in solution.

Principle of the experiment and theory

Three components, **R**, $\mathscr{R}$, and **P**, are submitted to the reaction

$$\mathbf{R} + \mathscr{R} \rightleftarrows \mathbf{P} \tag{1}$$

with k_1 and k_2 as the forward and reverse rate constants, and $K = k_1/k_2$ as the associated thermodynamic constant. $\mathscr{R}$ is introduced in excess over **R** and **P** and has a constant uniform concentration. Under such conditions, reaction (1) reduces to the simple two-state exchange process between **R** and **P**

$$\mathbf{R} \rightleftarrows \mathbf{P} \tag{2}$$

with $k_1[\mathscr{R}]$ and k_2 as the forward and reverse rate constants. To measure simultaneously both kinetic constants, the reacting mixture contains, at equilibrium, rather similar concentrations of **R** and **P** ($K[\mathscr{R}] \approx 1$). This equilibrated mixture is continuously introduced by electrophoresis and/or electro-osmosis from a narrow channel into a wide chamber filled with a migration medium supplemented with $\mathscr{R}$, at the same concentration as in the injected solution (Fig. 1).

Using a current injection design,[7] a uniform electric field is generated in the chamber beyond a distance ℓ_0 which typically corresponds to the lateral periodicity of the microfluidic array. Thus, the **R** and **P** solutes migrate at constant velocities along x and diffuse in two dimensions. After a transient regime, one obtains a stationary reaction–migration–diffusion pattern which, once imaged by epifluorescence video microscopy, can be used to retrieve all the dynamic parameters relevant to describe reaction (1), whatever the respective brightness of **R** and **P**.

[a]*Ecole Normale Supérieure, Département de Chimie, UMR CNRS ENS UPMC Paris 6 8640, 24, rue Lhomond, F-75005 Paris, France. E-mail: Ludovic.Jullien@ens.fr; Tel: +33 1 44 32 33 33*
[b]*Laboratoire de Photonique et de Nanostructures, LPN-CNRS, Route de Nozay, 91460 Marcoussis, France. E-mail: charlie.gosse@lpn.cnrs.fr; Fax: +33 1 69 63 60 06; Tel: +33 1 69 63 61 55*
[c]*Université Pierre et Marie Curie Paris 6, Laboratoire de Physique Théorique de la Matière Condensée, UMR CNRS 7600, 4, place Jussieu, 75252 Paris Cedex 05, France. E-mail: anle@lptmc.jussieu.fr; Fax: +33 1 44 27 72 87; Tel: +33 1 44 27 72 90*

† Electronic supplementary information (ESI) available: The theoretical derivation of the expression of the Fourier transform of the concentrations in **R** and **P**; the extraction of the dynamic parameters from the stationary reaction–migration–diffusion pattern of the fluorescence signal; the independent determinations of the thermodynamic constant K, the rate constants k_1 and k_2, the diffusion coefficients d_R and d_P, and the velocities v_R and v_P; the experimental constraints to retrieve the kinetic information from the reaction-migration-diffusion pattern. See DOI: 10.1039/b805412f

‡ The HTML version of this article has been enhanced with colour images.

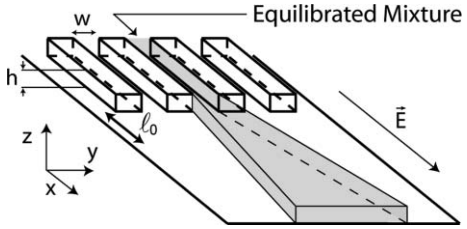

Fig. 1 Glass–PDMS chip layout for the continuous investigation of the dynamics of a reaction coupled with diffusion. A voltage drop along the x-axis is applied to introduce an equilibrated solution of interacting components from a narrow ($w = 20$ μm) and thin ($h = 10$ μm) injection channel into a wide (7.5 mm) square analysis chamber.[6] Inside the latter, the migration medium is subjected to a permanent and uniform electric field $\vec{E}$ parallel to the x-axis. After a transient regime, a stationary reaction–diffusion–migration pattern establishes. Hence, it is possible to average over time to improve the signal-to-noise ratio of the recorded image, which is advantageous for diluted or poorly fluorescent samples.

Because it is not simple to directly extract from the recorded pattern the respective contributions of the diffusive and reactive processes,[5,8] we perform a spatial Fourier transform along the y-direction. Indeed, such analysis gives access to the spatial dependence of the relaxation of the concentration profiles toward equilibrium and thus favours discrimination:[9] reaction (1) occurs homogeneously and its relaxation time does not depend on the spatial scale whereas the time scale for the relaxation by diffusion is inversely proportional to the square of the covered distance.

More precisely, to calculate the stationary reaction–migration–diffusion pattern (see the ESI† for details), we assume that the **R** and **P** motion occurs in a two-dimensional (2D) medium defined by ($0 \leqslant x \leqslant L$, $-\infty < y < +\infty$). This medium is submitted to a uniform constant electric field $\vec{E} = E\vec{u}_x$, where $\vec{u}_x$ is the unit vector along x. The diffusion coefficients of species **R** and **P** are respectively denoted d_R and d_P, their velocities (along the x-axis) v_R and v_P, and their concentration R and P. $\vec{E}$ is chosen to impose the migration of the averaged species {**R**,**P**} in the direction of increasing x. Considering at the ($x = 0$, $y = 0$) origin an {**R**,**P**} source associated with the equilibrium conditions $R(0,0)$ and $P(0,0)$, we look for stationary concentration profiles, $R(x,y)$ and $P(x,y)$, obeying the following partial differential equations:

$$-v_R\frac{\partial R(x,y)}{\partial x} + d_R\left[\frac{\partial^2 R(x,y)}{\partial x^2} + \frac{\partial^2 R(x,y)}{\partial y^2}\right] = k_1[\mathscr{R}]R(x,y) - k_2P(x,y) \quad (3)$$

$$-v_P\frac{\partial P(x,y)}{\partial x} + d_P\left[\frac{\partial^2 P(x,y)}{\partial x^2} + \frac{\partial^2 P(x,y)}{\partial y^2}\right] = -k_1[\mathscr{R}]R(x,y) + k_2P(x,y) \quad (4)$$

where $[\mathscr{R}]$ is assumed constant. After Fourier transform along y and restricting our analysis to a regime where diffusion along x can be neglected, eqns (3) and (4) lead to

$$\frac{\partial \tilde{R}(x,q)}{\partial x} = -\left(\delta_R q^2 + \kappa_1\right)\tilde{R}(x,q) + \kappa_2'\tilde{P}(x,q) \quad (5)$$

$$\frac{\partial \tilde{P}(x,q)}{\partial x} = \kappa_1'\tilde{R}(x,q) - \left(\delta_P q^2 + \kappa_2\right)\tilde{P}(x,q) \quad (6)$$

where $\tilde{R}(x,q) = 1/\sqrt{2\pi}\int_{-\infty}^{\infty} R(x,y)e^{-iqy}\,dy$, $\tilde{P}(x,q) = 1/\sqrt{2\pi}\times\int_{-\infty}^{\infty} P(x,y)e^{-iqy}\,dy$, $\kappa_1 = k_1[\mathscr{R}]/v_R$, $\kappa_1' = \kappa_1 v_R/v_P$, $\kappa_2 = k_2/v_P$, $\kappa_2' = \kappa_2 v_P/v_R$, $\delta_R = d_R/v_R$, and $\delta_P = d_P/v_P$. From eqns (5) and (6) the expressions of the Fourier transforms along y of the concentrations of **R** and **P** can be calculated analytically. It then yields the corresponding Fourier transform of the stationary reaction–migration–diffusion pattern of the fluorescence signal, $\tilde{F}$, which exhibits a simple bi-exponential dependence on the distance x (see ESI†):

$$\tilde{F} = F_+\exp(\lambda_+ x) + F_-\exp(\lambda_- x) \quad (7)$$

where the eigenvalues obey:

$$\lambda_\pm = -\frac{1}{2}\left[(\kappa_1+\kappa_2) + (\delta_R+\delta_P)q^2\right] \pm \frac{1}{2}\sqrt{\left[(\kappa_1+\kappa_2) + (\delta_R-\delta_P)q^2\right]^2 + 4(\delta_P-\delta_R)q^2\kappa_2} \quad (8)$$

The amplitude terms, F_+ and F_-, as well as the relaxation rates, λ_+ and λ_-, depend on the spatial frequency q along y and on the four dynamic parameters sought for: d_R, d_P, k_1, and k_2. Moreover, F_+ and F_- also depend on the shape of the concentration profile at the entry of the measurement chamber and on the relative brightness of **P** with regard to **R**. We demonstrate here that fitting the experimental data with eqns (7) and (8) yields d_P, k_1, and k_2, provided that d_R is known.

Materials and methods

Chemicals and solutions

Fluorescein, Hepes [4-(2-hydroxyethyl)-1-piperazineethanesulfonic acid], $Mg(OH)_2$, and 1 M NaOH solution were purchased from Sigma-Aldrich (Saint-Louis, MO). Low molecular weight DNA from salmon sperm was purchased from Fluka (St-Quentin Fallavier, France). Single-stranded oligonucleotides tex-9 (Texas-red-labeled in the 5′-position), U13, M100, and C100, respectively 9, 13, 100, and 100 bases long, were synthesized and HPLC-purified by IBA (Göttingen, Germany; sequences given in Table 1). Poly(dimethylacrylamide) (PDMA) of average molecular weight 3 MDa was a kind gift of J. Weber (Institut Curie, Paris, France).

Solutions were prepared using water purified through a Direct-Q 5 (Millipore, Billerica, MA). The 1 mg mL^{-1} stock solution of salmon sperm DNA was sonicated for 15 min and stored at 4 °C. Stock solutions of oligonucleotides (100 μM) were dissolved in 25/50 mM NaOH/Hepes pH 7.5 buffer and quantified by absorption measurements at 260 nm using a Uvikon-940 spectrophotometer (Kontron Instruments; T = 20 °C) and the absorption coefficients given by the manufacturer.

On-chip measurements

Epifluorescence imaging of the Texas-red-labeled reacting mixture was performed on a home-made microscope equipped with a set of filters (excitation HQ580/20x, dichroic Q595LP, emission HQ630/60m; Chroma Technology, Rockingham, VT),

Table 1 Sequences (5′–3′ orientation) of the oligonucleotides used in this study. Complementary sequences between tex-9 and M100 are shown in bold. Complementary sequences between U13 and M100 are underlined. Tex-9 perfectly hybridizes with the nine base-long sequence of C100 which is emphasized in italic

Name	Sequence
Tex-9	Texas-red-**CTTTGTTTG**
U13	TCCTTTGTTTGTG
M100	TAGTATTATCTTACATAAACAAAGGAGAATAAAA-TGAAAACGATTAATCTGAACGCTGCAGTTAAAA-CTAAATGCTTCAATGGTAAATATGATGAAACTA
C100	TAGTATTATCTTACA*CAAACAAAG*GAGAATAAAA-TGAAAACGATTAATCTGAACGCTGCAGTTAAAA-CTAAATGCTTCAATGGTAAATATGATGAAACTA

a 10× objective (Fluar NA 0.5; Zeiss, Le Pecq, France), and a CCD camera (CV-M4 + CL 2/3 in.; JAI, Copenhagen, Denmark). When needed, fluorescein emission was observed using a second set of filters (excitation HQ 495/30, dichroic 520 DCXR, emission HQ 560/80m; Chroma). Temperature was controlled at 20 °C with a thermostated microscope stage.

The chip and its detailed microfabrication protocol have been described in our previous work.[6] Briefly, the device is composed of two polydimethylsiloxane (PDMS) layers plasma-bonded to a circular glass coverslip. In the bottom layer, the square analysis chamber is 7.5 mm long and 10 μm high. The two opposite sides of the chamber are connected to a series of reservoirs through arrays of 20 μm wide microfluidic channels, separated by 20 μm wide walls. On one side (corresponding to negative x), a portion of the microchannels is bent to bring out a central injection channel connected to a 2 μL sample reservoir. The top PDMS layer is used to shape two 400 μL macroreservoirs accommodating the electrodes. This two-level design allows both small sample reservoirs in the bottom layer to reduce analyte consumption and large buffer reservoirs in the top layer to keep the pH constant during the experiment.

After assembly, the device was kept at 50 mbar for 45 min and subsequently filled with 55 mM Hepes buffer, pH 7.5, containing 25 mM Na^+, 1.25 mM Mg^{2+}, and 0.1% (w/w) polydimethylacrylamide (PDMA). PDMA smooths electroosmosis, thus reducing the dispersion that could be detrimental to extracting the diffusion coefficients. In contrast, it does not interfere with the association process at the corresponding concentration.

The tex-9 + M100 equilibrated mixture (1 μL) was then loaded in the sample reservoir while 10 μL of M100 solution were loaded in each of the two side reservoirs. We consequently ensured a homogeneous M100 concentration in the analysis chamber throughout the experiment. Note that all the loaded solutions contained 10% (v/v) glycerol, to prevent dilution in the buffer reservoir of the top PDMS layer, and 1 μM of fluorescein, to track the homogeneous filling of the whole device by M100.

A 600 V voltage drop was subsequently applied, resulting in a 1.6×10^4 V m^{-1} electric field along x. The fluorescent equilibrated mixture entered the analysis chamber and created a stationary concentration pattern that was recorded by video microscopy for 20 s. After averaging and fluorescence background subtraction, the image was Fourier transformed along y to obtain a bundle of 4–6 Fourier modes, depending on the experimental conditions. Each Fourier mode was subsequently normalized by the zero-frequency mode[6] and the resulting set of curves fitted as a whole by implementing eqns (7) and (8) in Igor Pro 5.0 (WaveMetrics, Lake Oswego, OR). The parameter δ_R was manually introduced in the fitting equation after d_R and v_R had been measured on the chip during an independent experiment.[6] Consequently, the fitting parameters were here $(\kappa_1 + \kappa_2)$, κ_2, δ_P, and F_+ (one has $F_- = 1 - F_+$).

Bulk titration experiments

Fluorescence measurements were performed on an LPS 220 spectrofluorimeter (Photon Technology International, Birmingham, NJ) in 25/50 mM NaOH/Hepes, 1.25/5 mM $Mg(OH)_2$/Hepes buffer, pH 7.5, supplemented with 10 μg mL^{-1} sonicated DNA salmon sperm, to prevent oligonucleotide adsorption, and 0.1% (w/w) PDMA (T = 20 °C). A quartz cuvette with a 1 cm optical path length was used. Excitation and emission wavelengths were respectively set at 587 and 612 nm with a bandwidth of 4 nm. After each experiment, the cuvette was cleaned for 15 min with 1% (v/v) Hellmanex soap (Hellma, Mülheim, Germany) in an ultrasonic bath.

Thermodynamic measurements. First, 400 μL of 50 nM tex-9 were equilibrated at 20 °C. The decrease in fluorescence intensity, associated with the hybridisation process, was then recorded while increasing concentrations of M100 were added at constant tex-9 concentration (Fig. 1S, ESI†). Data were finally analysed on the basis of reaction (1), for which the following formula can be easily obtained:

$$\frac{I_{eq}}{I_0} = 1 - \frac{1}{2}(1-Q)\left\{\left(1+\xi+\frac{1}{KR_0}\right) - \sqrt{\left(1+\xi+\frac{1}{KR_0}\right)^2 - 4\xi}\right\} \quad (9)$$

where I_{eq} is the fluorescence intensity at equilibrium when $\xi = \mathscr{R}/R_0$ equivalents of species $\mathscr{R}$ (*i.e.* M100) have been added, I_0 is the intensity at the beginning of the experiment, R_0 the initial concentration in tex-9, and Q the relative brightness of the duplex with regard to the free 9mer. R_0 being known, we extracted the thermodynamic constant, K, and Q by a least-squares fit.

Kinetic measurements. Using an RX2000 rapid kinetic stopped-flow accessory (Applied Photophysics, Leatherhead, UK), A and B solutions, 200 μL each, were mixed with a typical dead time of 100 ms and the fluorescence intensity was recorded over time at either 10 or 100 Hz. In dissociation experiments, solution A contained an equilibrated mixture of tex-9 + M100 (final concentrations 50 nM and 10 μM, respectively) and solution B an unlabeled oligonucleotide having an affinity for M100 much stronger than tex-9 (U13, final concentration 50 μM). In association experiments, solution A contained tex-9 and solution B M100 (final concentrations 50 nM and 10 μM, respectively). Once the k_2 value had been extracted by least-squares fitting of the dissociation curve, it was used to compute k_1 from the association experiment relaxation time.

Model for association experiments. The association reaction (1) reduces to (2) when $\mathscr{R}$ is in excess with respect to **R**. The characteristic time of the chemical reaction, τ, can thus

be written $\tau = (k_1[\mathscr{R}] + k_2)^{-1}$ and can be obtained using the expression

$$\frac{I(t)}{I_0} = \frac{I_{eq}}{I_0} + \left(1 - \frac{I_{eq}}{I_0}\right) e^{-t/\tau} \quad (10)$$

where $I(t)$ is the time-dependent fluorescence intensity.

Model for dissociation experiments. To determine k_2, we performed displacement experiments in which the unlabeled oligonucleotide U13 hybridises with M100 ($\mathscr{R}$) and takes the place of tex-9 (**R**) in the fluorescent duplex **P**. It consequently yields the much more stable non-fluorescent duplex $\mathbf{P_{NF}}$ (the corresponding kinetic scheme is detailed in the ESI†).

When the concentrations are chosen to make the dissociation of the fluorescent duplex **P** rate-limiting with regard to the subsequent formation of the non-fluorescent duplex $\mathbf{P_{NF}}$, the corresponding temporal evolution of the normalized fluorescence intensity is again given by eqn (10) but with $\tau = 1/k_2$.

Results

To evaluate the proposed approach for measuring dynamic parameters, we examine here the hybridisation between tex-9 (**R**), a fluorescent, Texas-red-labeled 9mer DNA oligonucleotide, and M100 ($\mathscr{R}$), a non-fluorescent 100mer (Scheme 1). Pairing of the complementary sequences (see Table 1) yields the corresponding fluorescent dsDNA (**P**).

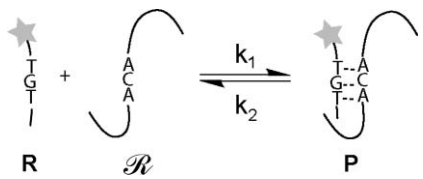

Scheme 1 Hybridisation between a rapidly diffusing oligonucleotide (tex-9; **R**) and its complementary target (M100; $\mathscr{R}$), yielding the corresponding slowly diffusing dsDNA (**P**).

The stationary reaction–migration–diffusion pattern resulting from the continuous introduction of an equilibrated mixture of **R** (1 μM) and $\mathscr{R}$ (10 μM) into the measurement chamber is shown in Fig. 2a. As anticipated, the signal profile associated with the fluorescent species **R** and **P** decreases and enlarges when the distance x from the injection nozzle increases.

Fig. 2b displays the discrete Fourier transform along y of the Fig. 2a video signal.[6] The resulting bundle of curves – the Fourier modes of the fluorescence signal $\tilde{F}$ – reflects, for different spatial frequencies, the relaxation of the fluorescence profile along y as a function of the distance x. Dynamic information is extracted from the q-dependence of λ_+ and λ_- after a global bi-exponential fit of the decays displayed in Fig. 2b. This analysis is performed only where the electric field is uniform, beyond the distance ℓ_0, and just three input parameters are required: d_R, v_R, and the average velocity of the exchanging **R** and **P** states v_{RP} (see ESI†). The first two (or similarly d_R and the **R** mobility μ_R) were measured in a preliminary experiment: as in ref. 6, a solution of pure **R** was injected into the same microsystem filled with pure buffer and the Fourier analysis of the migration–diffusion pattern yielded: $d_R = 153 \pm 10$ μm^2 s^{-1} and $\mu_R =$

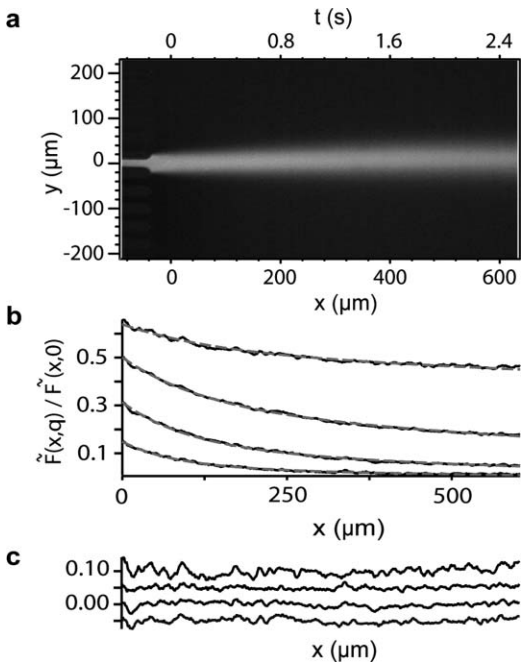

Fig. 2 (a) Reaction–migration–diffusion pattern obtained by continuous injection of a 1 μM tex-9 (**R**) + 10 μM M100 ($\mathscr{R}$) equilibrated mixture in a device filled with 10 μM M100 in 55 mM Hepes buffer, pH 7.5, containing 25 mM Na^+, 1.25 Mg^{2+}, and 0.1% (w/w) PDMA ($T = 20$ °C). The distance along x was converted into time using $x = v_{RP}t$, where v_{RP} designates the average velocity of the exchanging **R** and **P** states (here 250 μm s^{-1}). Transient time was approx. 3 s and images were accumulated during 20 s, yielding a complete experiment performed in 23 s. (b) Spatial dependency and global fit of the 1–4 normalized Fourier modes which result from the Fourier transform along y of the preceding image. The length scales along y associated with the Fourier modes are respectively $q^{-1} = 34$, 17, 12, and 9 μm. (c) Fit residuals. Offsets were introduced for a better readability.

$(20 \pm 2) \times 10^{-9}$ m^2 V^{-1} s^{-1} (see ESI†). The last parameter, v_{RP} (or correspondingly μ_{RP}), was measured during the present experiment by recording the progress into the analysis chamber of the equilibrated mixture fluorescent front. We derived $\mu_{RP} = (20 \pm 2) \times 10^{-9}$ m^2 V^{-1} s^{-1}. Equipped with the values of d_R, v_R, and v_{RP}, we obtained from the bi-exponential fit of the Fourier modes: $k_1 = (1.1 \pm 0.1) \times 10^5$ M^{-1} s^{-1}, $k_2 = (4.8 \pm 0.5) \times 10^{-1}$ s^{-1} [$k_1/k_2 = (2.3 \pm 1) \times 10^5$ M^{-1}], and $d_P = 39 \pm 4$ μm^2 s^{-1}.Values extracted from a second experiment performed at 3 μM in $\mathscr{R}$ were in agreement (Table 2).

Control bulk titration experiments, relying on fluorescence emission, were used to independently extract the thermodynamics and the kinetics of the tex-9/M100 hybridisation. We obtained $k_1 = (1.9 \pm 0.1) \times 10^5$ M^{-1} s^{-1}, $k_2 = (4.2 \pm 0.1) \times 10^{-1}$ s^{-1} [$k_1/k_2 = (4.5 \pm 0.3) \times 10^5$ M^{-1})], and, for the hybridisation thermodynamic constant, $K = (3.4 \pm 0.6) \times 10^5$ (M^{-1}). The difference between the bulk titration and the on-chip values are slightly outside error bars (see Table 2). Beyond different experimental conditions (concentrations, surface-to-volume ratios), we estimate that this observation could also originate from the less constrained analysis used for on-chip measurements: three parameters are extracted from multiple bi-exponential fits whereas each mono-exponential titration curve provides a single parameter. Finally, we independently estimated

Table 2 Extensive set of the dynamic parameters, k_1 (M^{-1} s^{-1}), k_2 (s^{-1}), and d_P (μm^2 s^{-1}), which characterises the hybridisation between tex-9 (**R**) and M100 ($\mathscr{R}$). The extracted k_1/k_2 ratio (M^{-1}) was compared with the equilibrium constant value K. All experiments were performed at 20 °C in 55 mM Hepes buffer, pH 7.5, containing 25 mM Na^+, 1.25 mM Mg^{2+}, and 0.1% (w/w) PDMA. For the on-chip experiments, an **R** + $\mathscr{R}$ equilibrated solution was continuously injected in the analysis chamber containing $\mathscr{R}$ at the same concentration; **R** was always at 1 μM whereas two different conditions were tested for $\mathscr{R}$, either 3 or 10 μM

Experiments	$10^{-5}k_1$	k_2	d_P	$10^{-5}k_1/k_2$	$10^{-5}K$
On-chip 3 μM	1.5 ± 0.1	0.37 ± 0.05	36 ± 3	4.0 ± 1	—
On-chip 10 μM	1.1 ± 0.1	0.48 ± 0.05	39 ± 4	2.3 ± 1	—
Bulk titration	1.9 ± 0.1	0.42 ± 0.01	—	4.5 ± 0.3	3.4 ± 0.6
On-chip control	—	—	40 ± 4	—	—

d_P by Fourier analysis of the tex-9 + C100 non-reactive mixture,[6] C100 being an M100 analog yielding a kinetically inert duplex. We derived[6] $d_P = 40 \pm 4$ μm^2 s^{-1}, in agreement with the value extracted from the above bi-exponential fit for the reactive mixture (see ESI†).

Discussion

As demonstrated, the present integrated approach satisfactorily yields thermodynamic, kinetic, and diffusion parameters involved in molecular associations. However, similarly to FCS, FRAP, or other microsystem-based measurements, it also admits some experimental constraints:

(i) To retrieve the kinetic information from the reaction–diffusion–migration pattern, it is necessary to fulfil the $(k_1[\mathscr{R}]/v_R + k_2/v_P) \approx (d_R/v_R - d_P/v_P)q^2$ condition for which the two processes, *i.e.* reaction (1) and diffusion, equally contribute to the relaxation of the concentration profiles toward equilibrium. Indeed, the mixture of **R** and **P** seems non-reactive if diffusion at the spatial frequency q dominates the reaction. In contrast, it behaves like a single species when reaction predominates over diffusion. Whatever the diffusion coefficients of the analytes, changing the voltage driving the motion of the solutes will therefore be the relevant strategy to access the range of spatial frequencies that focuses on kinetics.

(ii) In this study, we accessed the chemical relaxation time in the second range ($\tau \approx 1/2k_1[\mathscr{R}] \approx 1/2k_2$). By reducing the width of the injection channel and enlarging the microscope objective magnification, to permit observation at shorter spatial scales, one should easily perform measurements down to the 1–10 ms range.

(iii) To reliably measure λ_+ and λ_-, the amplitude terms F_+ and F_- have to be non-vanishing. It results in the $K[\mathscr{R}] \approx 1$ condition usually encountered in titration experiments. An appropriate camera detecting nanomolar concentrations in **R** and **P** should then make it possible to investigate reactions with association constants K up to 10^8 (M^{-1}).

Conclusion

We propose an attractive, new, integrated approach to analyse assembly formations in solution. It is easy to implement, rapid, and requires only a tiny amount of sample (1 pmol loaded in the injection well). Moreover, the assay is homogeneous, which allows any of the grafting procedures essential to numerous biosensors (*e.g.* Surface Plasmon Resonance) to be bypassed. Finally, with a minimum *a priori* knowledge of the analytes, an extensive set of thermodynamic, kinetic, and diffusion parameters ruling the association can simply be derived from a global, robust, bi-exponential fit. These features correspondingly make the present continuous technique appropriate for pharmaceutical and biological applications.

Acknowledgements

We thank J.-L. Mergny, L. Lacroix, V. Croquette, J.-F. Allemand, and H. Berthoumieux for insightful discussions. This work was supported by the ACN 2003 'Cargos Moléculaires' and ACI-NMAC 2003 'Puces Cinétiques' grants from the Ministère de la Recherche et de la Technologie (to L. J., C. G., and A. L.) and a Ministère de la Recherche fellowship (to A. E. T.).

References

1 C. R. Cantor and P. R. Schimmel, *Biophysical Chemistry: Part II: Techniques for the Study of Biological Structure and Function*, Freeman, New York, 1980.
2 S. Charier, A. Meglio, D. Alcor, E. Cogné-Laage, J.-F. Allemand, L. Jullien and A. Lemarchand, *J. Am. Chem. Soc.*, 2005, **127**, 15491–15505; D. Alcor, V. Croquette, L. Jullien and A. Lemarchand, *Proc. Natl. Acad. Sci. U. S. A.*, 2004, **101**, 8276–8280.
3 E. L. Elson and D. Magde, *Biopolymers*, 1974, **13**, 1–27; D. Magde, E. L. Elson and W. W. Webb, *Biopolymers*, 1974, **13**, 29–61.
4 D. Axelrod, D. E. Koppel, J. Schlessinger, E. Elson and W. W. Webb, *Biophys. J.*, 1976, **16**, 1055–1069; D. E. Koppel, D. Axelrod, J. Schlessinger, E. Elson and W. W. Webb, *Biophys. J.*, 1976, **16**, 1315–1329.
5 A. E. Kamholz, B. H. Weigl, B. A. Finlayson and P. Yager, *Anal. Chem.*, 1999, **71**, 5340–5347; J.-B. Salmon, C. Dubrocq, P. Tabeling, S. Charier, D. Alcor, L. Jullien and F. Ferrage, *Anal. Chem.*, 2005, **77**, 3417–3424.
6 A. Estévez-Torres, C. Gosse, T. Le Saux, J.-F. Allemand, V. Croquette, H. Berthoumieux, A. Lemarchand and L. Jullien, *Anal. Chem.*, 2007, **79**, 8222–8231.
7 L. R. Huang, J. O. Tegenfeldt, J. J. Kraeft, J. C. Sturm, R. H. Austin and E. C. Cox, in *IEDM Technical Digest 2001: International Electron Devices Meeting*, ed. IEEE, Electron Devices Society Staff, IEEE, Piscataway, NJ, 2001, pp. 363–366.
8 B. L. Sprague, R. L. Pego, D. A. Stavreva and J. G. McNally, *Biophys. J.*, 2004, **86**, 3473–3495.
9 D. A. Berk, F. Yuan, M. Leunig and R. K. Jain, *Proc. Natl. Acad. Sci. U. S. A.*, 1997, **94**, 1785–1790.